A paradigm of thermal adaptation in penguins and elephants by tuning cold activation in TRPM8

Shilong Yang[a,b,1], Xiancui Lu[a,c,1], Yunfei Wang[a,b,1], Lizhen Xu[d,1], Xiaoying Chen[d], Fan Yang (杨帆)[d,2], and Ren Lai[a,e,f,g,h,2]

[a]Key Laboratory of Animal Models and Human Disease Mechanisms of the Chinese Academy of Sciences/Key Laboratory of Bioactive Peptides of Yunnan Province, Kunming Institute of Zoology, Chinese Academy of Sciences, 650223 Kunming, Yunnan, China; [b]College of Wildlife and Protected Area, Northeast Forestry University, 150040 Harbin, China; [c]College of Life Sciences, University of Chinese Academy of Sciences, 100049 Bejing, China; [d]Department of Biophysics and Kidney Disease Center, First Affiliated Hospital, Institute of Neuroscience, National Health Commission and Chinese Academy of Medical Sciences Key Laboratory of Medical Neurobiology, Zhejiang University School of Medicine, 310058 Hangzhou, Zhejiang, China; [e]Kunming Institute of Zoology–Chinese University of Hong Kong Joint Laboratory of Bioresources and Molecular Research in Common Diseases, Kunming Institute of Zoology, Chinese Academy of Sciences, 650223 Kunming, Yunnan, China; [f]Sino-African Joint Research Center, Kunming Institute of Zoology, Chinese Academy of Sciences, 650223 Kunming, Yunnan, China; [g]Center for Biosafety Mega-Science, Chinese Academy of Sciences, 430071 Wuhan, Hubei, China; and [h]Institute for Drug Discovery and Development, Chinese Academy of Sciences, 201203 Shanghai, China

Edited by David E. Clapham, Howard Hughes Medical Institute, Ashburn, VA, and approved March 3, 2020 (received for review December 26, 2019)

To adapt to habitat temperature, vertebrates have developed sophisticated physiological and ecological mechanisms through evolution. Transient receptor potential melastatin 8 (TRPM8) serves as the primary sensor for cold. However, how cold activates TRPM8 and how this sensor is tuned for thermal adaptation remain largely unknown. Here we established a molecular framework of how cold is sensed in TRPM8 with a combination of patch-clamp recording, unnatural amino acid imaging, and structural modeling. We first observed that the maximum cold activation of TRPM8 in eight different vertebrates (i.e., African elephant and emperor penguin) with distinct side-chain hydrophobicity (SCH) in the pore domain (PD) is tuned to match their habitat temperature. We further showed that altering SCH for residues in the PD with solvent-accessibility changes leads to specific tuning of the cold response in TRPM8. We also observed that knockin mice expressing the penguin's TRPM8 exhibited remarkable tolerance to cold. Together, our findings suggest a paradigm of thermal adaptation in vertebrates, where the evolutionary tuning of the cold activation in the TRPM8 ion channel through altering SCH and solvent accessibility in its PD largely contributes to the setting of the cold-sensitive/tolerant phenotype.

TRPM8 | cold activation | pore domain | side-chain hydrophobicity | thermal adaptation

To survive and thrive, all living beings have to perceive and adapt to ambient temperature (1), which varies over a wide range from below −50 °C in polar areas to above 50 °C in deserts (2). Therefore, sophisticated physiological and ecological mechanisms have been developed through evolution to first detect and then adapt to ambient temperature (3–5). The transient receptor potential melastatin 8 (TRPM8) channel is the prototypical sensor for cold in vertebrates (6, 7), which has been validated in both knockout mice (8) and pharmacological studies (9). However, how cold activates TRPM8 remains obscure. From the perspective of channel structure, an earlier study suggested that its C terminus is crucial for cold activation (10), while subsequent work demonstrated that the transmembrane core domain (5) or the pore domain (11) is essential for setting cold response. Although high-resolution structures of TRPM8 have been resolved by cryoelectron microscopy in both the apo and ligand-bound states (12–14), its cold-activated state structure is still unavailable. From the perspective of thermodynamics, large enthalpic (ΔH) and entropic (ΔS) changes are associated with TRPM8 cold activation (15, 16). Changes in heat capacity have also been hypothesized to mediate cold activation (17), though experimental evidence for such a hypothesis is limited to voltage-gated potassium channels (18). Interestingly, cold activation of TRPM8 is tuned during evolution in several tested vertebrate species (5, 11, 19). To understand both the structural and thermodynamic bases of TRPM8 cold activation, we attempted to gain insights from TRPM8 orthologs in vertebrate species inhabiting distinct ambient temperatures.

Results

TRPM8 Cold Activation Correlates with Habitat Temperature. We first measured maximum cold activation compared with saturated menthol (1 mM) activation in TRPM8 orthologs (Fig. 1 *A* and *B* and *SI Appendix*, Table S1). In TRPM8_LA (the TRPM8 of the African elephant *Loxodonta africana*), we observed that cooling to 6 °C elicited a robust activation that was at 84.3 ± 3.7% ($n = 5$) of menthol-induced activation, while the same cooling only activated a minute current level (14.8 ± 1.5% of menthol-induced activation; $n = 5$) in TRPM8_AF (the TRPM8 of the emperor penguin *Aptenodytes forsteri*). Such a distinction in maximum cold activation among TRPM8 orthologs prompted us to examine the relationship between the habitat temperature and TRPM8 channel of these species.

Significance

Sensing temperature is critical for the survival of all living beings. Here, we show that during cold-induced activation of the archetypical temperature-sensitive TRPM8 ion channel, there are hydrophobic residues in the pore domain stabilized in the exposed state. Tuning hydrophobicity of these residues specifically alters cold response in TRPM8. Furthermore, TRPM8 orthologs in vertebrates evolved to employ such a mechanism, which physiologically tunes cold tolerance for better thermal adaptation. Our findings not only advance the understanding of the cold-induced activation mechanism of TRPM8 but also bring insights to the molecular evolution strategy for ambient-temperature adaptation in vertebrates.

Author contributions: S.Y. and F.Y. designed research; S.Y., X.L., Y.W., L.X., X.C., and F.Y. performed research; S.Y., X.L., and Y.W. analyzed data; and S.Y., F.Y., and R.L. wrote the paper.

The authors declare no competing interest.

This article is a PNAS Direct Submission.

Data deposition: The sequencing data of mouse trigeminal ganglions reported in this paper have been deposited in the National Center for Biotechnology Information Sequence Read Archive (accession no. PRJNA600306).

[1]S.Y., X.L., Y.W., and L.X. contributed equally to this work.

[2]To whom correspondence may be addressed. Email: fanyanga@zju.edu.cn or rlai@mail.kiz.ac.cn.

This article contains supporting information online at https://www.pnas.org/lookup/suppl/doi:10.1073/pnas.1922714117/-/DCSupplemental.

First published March 27, 2020.

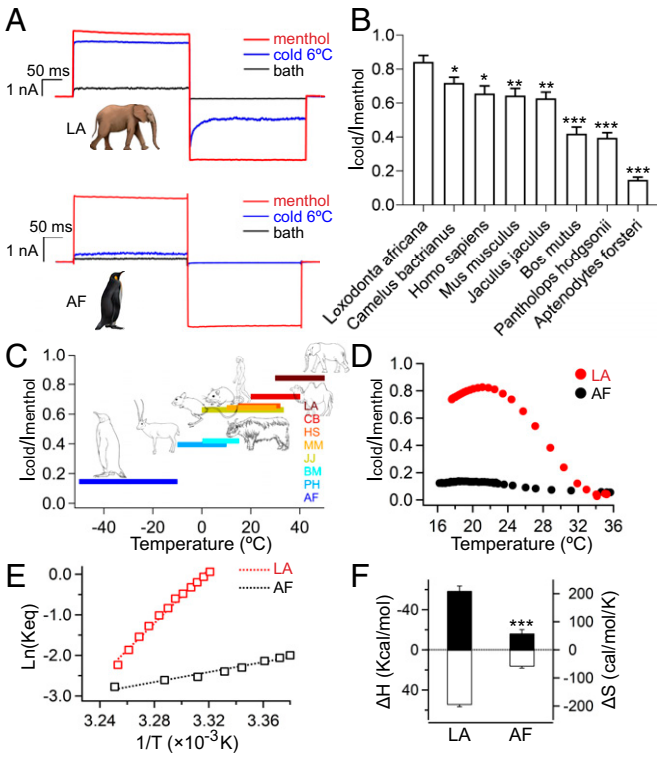

Fig. 1. TRPM8 channels in different species are distinct in cold activation. (*A*) Representative currents of TRPM8_LA and TRPM8_AF activated by cold (6 °C) and 1 mM menthol, respectively. (*B*) Comparison of the cold activation of eight TRPM8 orthologs. The maximum cold-activated current amplitudes were normalized to saturated menthol-induced activation. TRPM8 orthologs activated by 1 mM menthol served as maximum activation (mean ± SEM; $*P < 0.05$, $**P < 0.01$, $***P < 0.001$; $n = 5$). (*C*) The correlation between normalized cold responses of specific TRPM8 orthologs and their habitat temperatures (mean; $n = 5$). AF, *A. forsteri*; BM, *Bos mutus*; CB, *Camelus bactrianus*; HS, *Homo sapiens*; JJ, *Jaculus jaculus*; LA, *L. Africana*; MM, *Mus musculus*; PH, *Pantholops hodgsonii*. (*D*) Representative temperature-driven responses of TRPM8_LA and TRPM8_AF. The cold-activated currents were normalized to saturated menthol-induced activation. (*E*) Van't Hoff plots for the cold-activated TRPM8 currents shown in *D*. Dotted lines represent fits of the Van't Hoff equation, from which ΔH and ΔS are estimated. (*F*) Measured ΔH values (filled bars, left axis) and ΔS values (open bars, right axis) of TRPM8_LA and TRPM8_AF (mean ± SEM; $***P < 0.001$; $n = 5$).

We measured the cold activation of TRPM8 orthologs from vertebrate species covering a large habitat-temperature range. We observed that the maximum cold activation of these channels positively correlates with habitat temperature (Fig. 1*C*). The emperor penguin living in the Antarctic region and African elephant living in the Sahel desert showed the lowest and highest cold-activated currents, respectively, while other TRPM8 orthologs exhibited cold activation in-between (Fig. 1 *B* and *C* and *SI Appendix*, Fig. S1). Such results suggest that the cold activation of the TRPM8 channel is tuned for thermal adaptation. This encouraged us to perform a detailed functional analysis of thermodynamic parameters for TRPM8_LA and TRPM8_AF, of which the difference in habitat temperature is the largest, aiming to understand how cold activation is tuned.

To quantify the thermodynamics of cold activation in TRPM8, like the previous study (16), we measured the temperature–current relationship (Fig. 1*D*) and then calculated the temperature dependence of the equilibrium constant (K_{eq}) from Van't Hoff plots (Fig. 1*E*) to derive ΔH and ΔS changes, which are the slope and intercept of the plots, respectively. We observed that in addition to larger maximum cold-activation current, TRPM8_LA exhibited a much steeper temperature dependence of current (Fig. 1*E*) than TRPM8_AF, and therefore ΔH and ΔS of TRPM8_LA are much larger than those of TRPM8_AF (Fig. 1*F*). The cold activation of the TRPM8 channel was suggested to be affected by voltage gating (6, 16, 20), so we tested and found that these channels were very similar in voltage dependence (*SI Appendix*, Fig. S2). These results indicate that intrinsic cold-activation properties such as ΔH and ΔS are the primary factors for the difference in cold activation of TRPM8_LA and TRPM8_AF.

Site 919 Is Crucial for TRPM8 Cold Activation. To probe the origin of differences in ΔH and ΔS, we focused on nonconserved residues within the pore domain (PD) of TRPM8_LA and TRPM8_AF (Fig. 2*A*), because swapping domains outside the PD between these channels barely altered the cold activation (*SI Appendix*, Fig. S3 and Tables S2 and S3). By interchanging nonconserved residues with mutagenesis (Fig. 2*B*, *SI Appendix*, Fig. S4, and Datasets S1 and S2), we found that V919Y, a single-point mutation located in the pore helix of TRPM8_LA, significantly reduced the maximum cold-activation current, while in TRPM8_AF the reverse mutation (Y919V) increased cold activation (Fig. 2 *C* and *D*).

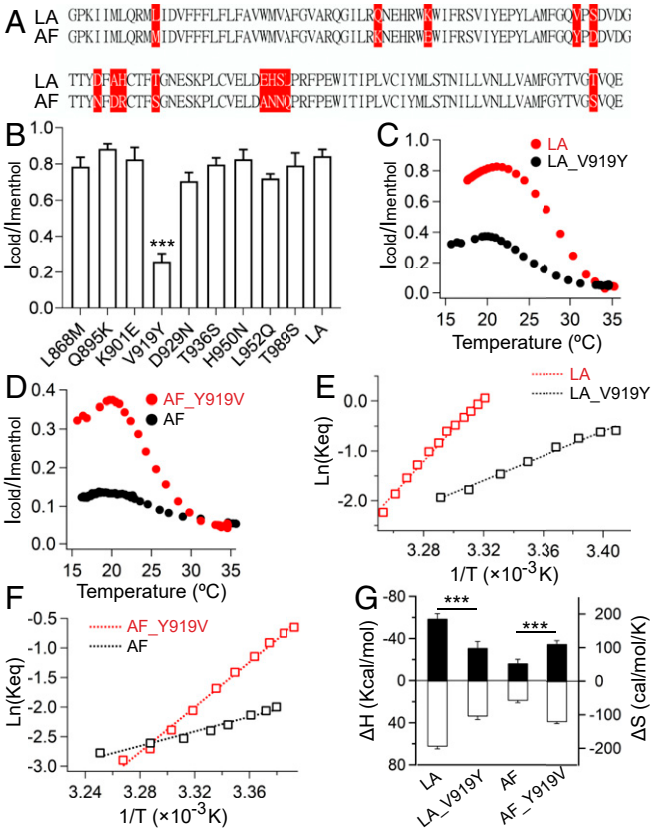

Fig. 2. Mutations at site 919 in the PD alter the thermodynamic properties of TRPM8 cold activation. (*A*) Sequence alignment of amino acids in the PD of TRPM8_LA and TRPM8_AF. The species-specific residues are highlighted. (*B*) Normalized maximum cold-activated currents of TRPM8_LA and its mutants. The cold-activated currents were normalized to saturated menthol-induced activation (mean ± SEM; $***P < 0.001$; $n = 5$). (*C*) Representative temperature-driven activation of wild-type TRPM8_LA and its V919Y mutant. (*D*) Representative temperature-driven activation of wild-type TRPM8_AF and its Y919V mutant. (*E*) Van't Hoff plots for the cold-activated TRPM8 currents shown in *C*. Dotted lines represent fits of the Van't Hoff equation. ΔH and ΔS were calculated directly from the slope and intercept of the plots. (*F*) Van't Hoff plots for the cold-activated TRPM8 currents shown in *D*. (*G*) Measured ΔH (filled bars, left axis) and ΔS values (open bars, right axis) of TRPM8_LA, TRPM8_AF, and the channel mutants (mean ± SEM; $***P < 0.001$; $n = 5$).

Furthermore, V919Y in TRPM8_LA decreased the ΔH and ΔS of cold activation, while Y919V in TRPM8_AF increased the ΔH and ΔS (Fig. 2 *E*–*G*). Therefore, our observations support the critical role of the TRPM8 PD in cold activation as mutations at site 919 significantly influence cold-activation properties.

Conformational States of Key Residues during Cold Activation. To reveal the general principle underlying changes in cold activation caused by such a single substitution, we first examined potential mutations that can alter thermodynamic properties of the host channels. Based on thermodynamic principles (17), it was hypothesized that change in channel protein-specific heat capacity (ΔCp) is associated with temperature gating of TRP channels, so when the side chain of a hydrophobic residue transits from buried state to water-exposed state, changes in ΔCp will be positive, leading to an increase in cold response (18). We intended to test whether our observations could be explained within such a molecular framework of temperature gating.

To test this hypothesis, two tasks were to be accomplished: 1) We needed to know the side chain of which residues undergo buried/exposed conformational changes during cold activation; and 2) for the residues changing buried/exposed states, we needed to systematically alter the side-chain hydrophobicity (SCH) and then measure the changes in cold response. To first probe buried/exposed conformational changes of the side chain, we employed an unnatural amino acid, 3-(6-acetylnaphthalen-2-ylamino)-2-aminopropanoic acid (ANAP) (Fig. 3*A*) (21). Given that the emission peak of ANAP shifts to a higher wavelength in more hydrophilic environments due to the changes in solvation of the side chains of ANAP-incorporated residues (21), we used it to monitor ligand- and heat-induced conformational rearrangements in the transient receptor potential vanilloid 1 (TRPV1) channel (22, 23). We incorporated ANAP at 142 sites throughout the transmembrane domains of TRPM8_LA (Datasets S3 and S4), where 15 ANAP-incorporated TRPM8 channels were still activated by cold. These functional ANAP-incorporated mutants allowed us to determine at least a set of residues with buried/exposed conformational changes in their side chains. Among these channels, we observed that three mutants (G925ANAP, L943ANAP, and L947ANAP) exhibited a significant red shift in their ANAP emission peak upon cold activation (Fig. 3 *B*–*F*), suggesting that these residues changed from buried to exposed state during cold activation. They showed similar single-channel conductance values and channel activation as the wild-type channel (*SI Appendix*, Figs. S5 and S6), indicating that ANAP incorporation did not disrupt ion permeation. As the selectivity filter remains virtually unobserved in cryoelectron microscopy structures of the collared flycatcher TRPM8 channel (12, 13), we computationally modeled the intact pore of TRPM8_LA with multiple rounds of kinematic loop modeling (*SI Appendix*, Fig. S7 *A* and *B*), where the pore radius at the selectivity filter turned out to be too narrow to allow ions and water molecules to pass (*SI Appendix*, Fig. S8*A*). We mapped the shifts in ANAP emission onto this closed-state model of TRPM8_LA and observed that these three sites with the largest shifts are clustered within the PD (Fig. 3*G*), which again supports the critical role of the PD in cold activation of the channel (5, 11).

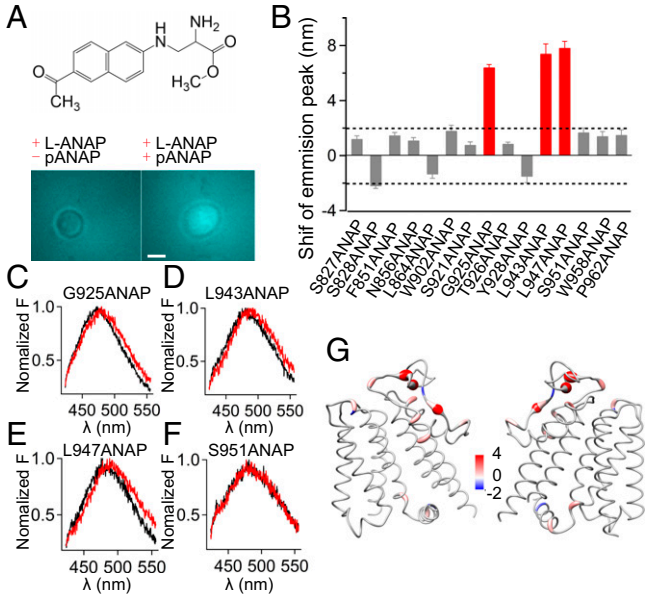

Fig. 3. Conformational state of key residues in the PD during TRPM8 cold activation. (*A*, *Top*) Chemical structure of ANAP. (*A*, *Bottom*) ANAP-incorporated TRPM8_LA channels were only expressed in HEK293 cells in the presence of the suppression plasmid (pANAP). Pseudocolors for ANAP are used. (Scale bar, 10 μm.) (*B*) Summary of the shifts in emission spectra of ANAP incorporated in TRPM8_LA (mean ± SEM; $n = 5$). The red bars indicate the ANAP emission spectra with significant changes during cold activation. (*C*–*F*) Representative ANAP emission spectra measured at low (6 °C) (red) and high temperature (30 °C) (black) for sites 925, 943, 947, and 951, respectively. (*G*) Shifts in the ANAP emission peak mapped onto the TRPM8_LA model with a worm representation, where the worm radius was proportional to the amplitude of shifts. Right and left shifts are colored in red and blue, respectively. (Scale bar, 6 nm.)

Side-Chain Hydrophobicity Alters Cold Response. Next, we systematically tuned the cold response of TRPM8_LA by introducing point mutations with varying SCHs at sites 925, 943, and 947 (Dataset S5), for which ANAP experiments have specified their buried/exposed conformational changes during cold activation (Fig. 3 *B*–*F*). Altering the SCH of these residues would tune the cold response of the channel in a predictable way. We expected that changing the amino acid to a more hydrophobic residue would increase cold response, while the substitution of a more hydrophilic residue would cause a decrease. To experimentally determine the hydrophobicity of ANAP, we further employed reverse-phase chromatography to compare the elution time of ANAP relative to natural amino acids. Leucine has been determined in different systems as one of the most hydrophobic amino acids (24–26). As expected, the elution time of leucine is longer than that of the hydrophilic glutamine. We observed that the elution time of ANAP was even longer than that of leucine, suggesting that ANAP is more hydrophobic than natural amino acids including leucine (Fig. 4*A*). For site 925, we measured the ΔH and ΔS of cold activation when its side chain was that of ANAP, isoleucine, glycine (wild type), or glutamine. With the increase in SCH by using ANAP or isoleucine, the ΔH and ΔS values were significantly increased; in contrast, the hydrophilic glutamine yielded decreased ΔH and ΔS (Fig. 4 *B* and *C*). The cold sensitivity (as indicated by ΔH values) positively correlated well with SCH (Fig. 4*B*). For the mutation at sites 943 and 947, we observed the same trend: An increase in SCH with ANAP led to greater cold sensitivity, while a decrease in SCH with lysine or glutamine reduced cold sensitivity (Fig. 4 *D*–G). Therefore, the molecular framework of temperature gating was supported by our observations at sites 925, 943, and 947.

Site 919 in TRPM8 Cold Activation. Unfortunately, when ANAP was incorporated at site 919 of TRPM8_LA, where a point mutation largely altered thermodynamic properties, the channel became unresponsive to cold and menthol stimuli (*SI Appendix*, Fig. S6), preventing direct measurement of conformational rearrangements in the side chain at this site during cold activation. To estimate how the buried/exposed state changes at site 919, we employed ANAP emission shifts as experimentally derived constraints to facilitate computational modeling of the cold-induced

PHYSIOLOGY

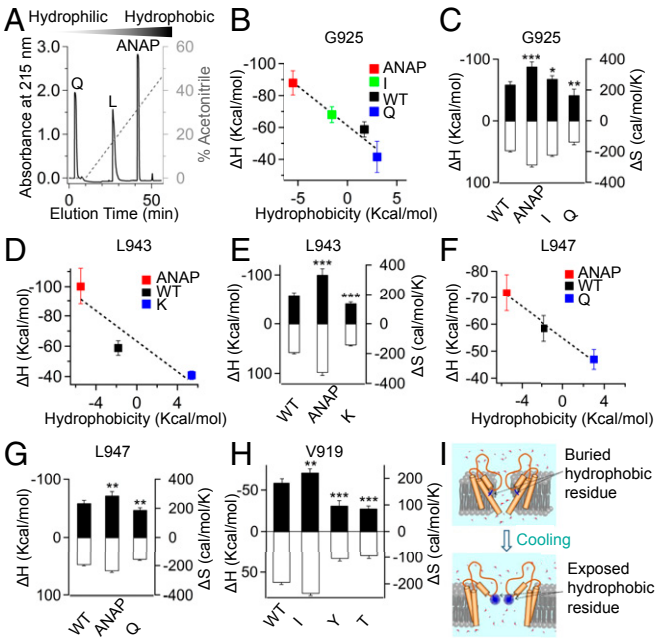

Fig. 4. SCH of residues located in the PD tunes the cold sensitivity of TRPM8. (*A*) Relative hydrophobicity of amino acids was compared by a C_{18} reverse-phase high-performance liquid chromatography column. (*B–G*) SCH of residues located in sites 925, 943, and 947 of TRPM8_LA positively correlates with the measured ΔH values. Measured ΔH values (filled bars, left axis) and ΔS values (open bars, right axis) of wild-type TRPM8_LA and channel mutants (mean ± SEM; $*P < 0.05$, $**P < 0.01$, $***P < 0.001$; $n = 5$). (*H*) Measured ΔH (filled bars, left axis) and ΔS values (open bars, right axis) of wild-type TRPM8_LA and its mutants with point substitution at site 919 (mean ± SEM; $**P < 0.01$, $***P < 0.001$; $n = 5$). (*I*) A schematic illustration where a hydrophobic residue transits from the buried (*Top*) to exposed state (*Bottom*).

open state. Briefly, a red shift in ANAP emission indicates that the solvent-accessible surface area (SASA) of its side chain is increased. Since SASA can be directly measured from the three-dimensional structure of the channel, we had previously used this strategy to computationally model the capsaicin-activated state and the heat-desensitized state of the TRPV1 channel (22, 23). With constraints and multiple rounds of kinematic loop modeling and relaxation in Rosetta (*SI Appendix*, Fig. S7 *C* and *D*), we modeled the cold-activated state of TRPM8_LA, where the pore radius at the selectivity filter was large enough for ion permeation (*SI Appendix*, Fig. S8*A*). By comparing TRPM8_LA structure models in the closed and cold-activated states, we observed an increased SASA of the V919 side chain during cold activation (*SI Appendix*, Fig. S8 *B* and *C*). We were aware that computational modeling was prone to inaccuracy despite the experimental constraints we employed here. Assuming SASA of the V919 side chain in TRPM8_LA was indeed increased during cold activation as suggested by our models, we further mutated valine to isoleucine, which made site 919 more hydrophobic. With patch-clamp recording, we observed that both ΔH and ΔS of the V919I mutant were significantly increased. In contrast, as threonine is much more hydrophilic than valine, the V919T mutant led to significantly reduced ΔH and ΔS (Fig. 4*H*). The V919Y mutant showed decreased cold sensitivity (Figs. 2*G* and 4*H*). Tyrosine, which preferably locates at the water–membrane interface (27–31), is an aromatic residue with a polar hydroxyl group on its side chain, which may make it hydrophobic in some studies (32–35) but hydrophilic in others (26, 36, 37). With all these complications, our observations of the V919I and V919T mutants support the molecular framework of temperature gating where both the buried/exposed state and SCH control the temperature sensitivity of TRPM8 (Fig. 4*I*).

Cold-Activation Properties of TRPM8 Contribute to Thermal Adaptation. Such a framework of temperature gating predicted that cold could induce similar conformational rearrangements in TRPM8 orthologs. Indeed, we observed that the accumulated SCH of the PD by summing up hydrophobicity values (24, 25) of nonconserved residues (*Materials and Methods*) positively correlated with both the habitat temperature of each species (Fig. 5 *A* and *B*) and the maximum cold activation of TRPM8 (Fig. 5*C*). Such a correlation prompted us to hypothesize that those changes in TRPM8 cold activation by tuning SCH likely serve as one of the mechanisms for thermal adaptation in vertebrate species.

To test this hypothesis, we first used the *trpm8* gene from the emperor penguin to replace that of mice by a transgenic approach (AF mice). AF mice showed normal physiological characteristics in blood tests (*SI Appendix*, Tables S5 and S6) and unchanged transcription levels of TRPM8 messenger RNA as well as other thermal sensing-related ion channels (*SI Appendix*, Fig. S9 *A* and *B*). As expected, TRPM8_AF channels were well-expressed in the trigeminal ganglion (*SI Appendix*, Fig. S9 *C–E*) and dorsal root ganglion (*SI Appendix*, Fig. S10) of AF mice, where these channels were still activated by menthol and cold (*SI Appendix*, Fig. S10).

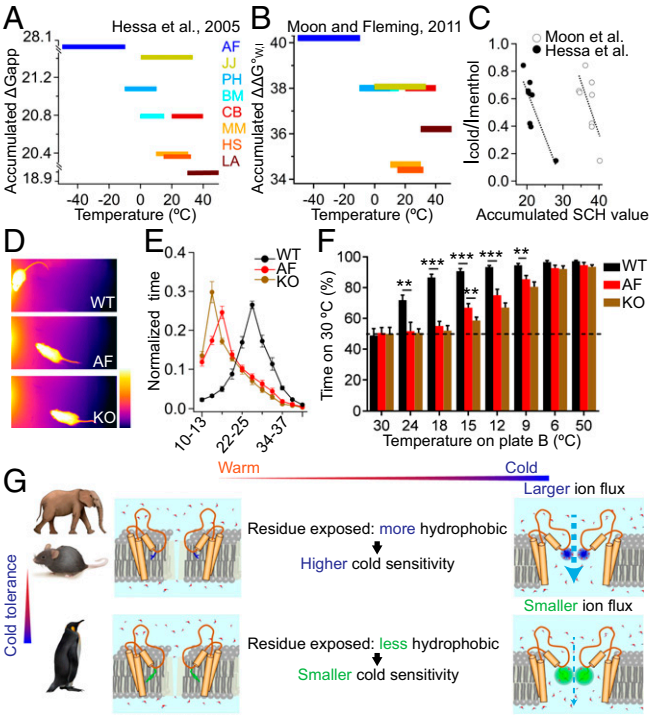

Fig. 5. Tuning of SCH serves as the adaptation strategy for habitat temperature. (*A* and *B*) The relationship between the accumulated SCH value of each TRPM8 ortholog's PD and the habitat temperature of each vertebrate. SCH values were taken from ref. 24 (*A*) or ref. 25 (*B*). (*C*) The relationship between the accumulated SCH value and the normalized cold response. (*D*) Images of mice at the comfortable position, indicating the favored temperature. KO, knockout. (Scale bar, 4 to 37 °C.) (*E*) The detention time of mice at each temperature area was normalized to the total time of the temperature-preference test. Average values represent mean ± SEM ($n = 10$). (*F*) Mice were allowed to move freely in a two-temperature choice test with control plate (30 °C) and test plate (ranging from 6 to 30 °C). The percentage of time spent at the control plate was measured every 3 min (mean ± SEM; $*P < 0.05$, $**P < 0.01$, $***P < 0.001$; $n = 10$). (*G*) A cartoon illustrating the molecular mechanism of TRPM8 cold-induced activation and thermal adaptation in vertebrates.

We observed that compared with wild-type mice (25 to 28 °C), both the AF mice (16 to 19 °C) and *trpm8*$^{-/-}$ knockout mice (13 to 16 °C) preferred a cooler temperature (Fig. 5 *D* and *E*). Similarly, unlike wild-type mice, AF mice were able to tolerate the cold temperature (9 to 24 °C) in the two-temperature choice tests (Fig. 5*F* and Movie S1). Although TRPM8-deficient mice exhibited equal ability to adapt to a cold environment compared with AF mice, other TRPM8-related physiological functions were compromised, such as response to chemical stimuli (8, 38, 39). Therefore, tuning cold-activation properties of the single-gene–encoded TRPM8 channel is likely the most efficient and low-cost strategy, which contributes to better adaptation of the emperor penguin and other vertebrates to their habitat temperature.

Discussion

In summary, we demonstrated that by first identifying the residues with their side chains that undergo buried/exposed conformational rearrangements with ANAP imaging, we could specifically increase or decrease the cold sensitivity (as indicated by ΔH) of the TRPM8 channel by making these residues more hydrophobic or hydrophilic, respectively (Fig. 4). The TRPM8 channel is an allosteric protein where stimulus-sensing apparatuses are energetically coupled to the activation gate like in other TRP channels (40, 41), so the maximum cold activation is determined by the equilibrium constant of the channel gate itself (42, 43). As we also observed that maximum cold activation is tuned similarly as cold sensitivity (Figs. 2 *C*–*G* and 5*C*) and the channel gate is located within the PD (12–14), we suggested that in agreement with previous reports (5, 11), the TRPM8 PD is critical for cold-activation properties, which may be involved as part of the cold-sensing apparatus. Accordingly, the PD in TRPV1 and TRPV3 has also been shown to be critical for heat activation (15, 44–46). However, for site 919 in particular, where mutations largely altered cold activation in TRPM8 orthologs (Fig. 2 *C*–*G*), there are several possibilities regarding its specific role in temperature-gating mechanisms: 1) The PD may contain a temperature sensor with site 919 acting as part of the upper gate, though whether the selectivity filter serves as a gate for ion permeation needs to be further tested (47); 2) site 919 may be a modulatory site while the actual "temperature sensor" is located elsewhere; and 3) site 919 is part of a scattered but somewhat coordinated group of residues "sensing" temperature as proposed in a previous study (17). Because we observed that tuning the SCH of other sites (925, 943, and 947) in the PD also specifically tuned the cold sensitivity in TRPM8 (Fig. 4), site 919 is more likely to be part of a scattered but somewhat coordinated group of residues sensing temperature, though further experiments are required to establish the roles of these residues.

Given that the hydration shell formed by water molecules surrounding the exposed hydrophobic side chain is more stable at lower temperatures (18), we postulated a temperature-gating mechanism where cold makes the exposed state of hydrophobic residues in the PD be energetically favorable, leading to the opening of activation gate inside the PD. In contrast to TRPM8, TRPV1 is activated by noxious heat. Based on high-throughput mutagenesis, it has been shown that TRPV1 heat activation is specifically sensitive to strong decreases in amino acid hydrophobicity (48), which is in agreement with the temperature-sensing framework we proposed. In some vertebrates, though the transient receptor potential ankyrin 1 (TRPA1) channel has been suggested to detect cold (49, 50), TRPM8 is still the most established cold sensor. Therefore, such a molecular framework of temperature gating has also been employed in an evolutionary paradigm where cold-activation properties in TRPM8 orthologs are tuned with the SCH of residues in the PD for better thermal adaptation in vertebrates (Fig. 5*G*).

Materials and Methods

Animals. All experiments involving animals conformed to the recommendations in the Guide for the Care and Use of Laboratory Animals of the Kunming Institute of Zoology, Chinese Academy of Sciences. All experimental procedures were approved by the Institutional Animal Care and Use Committees at the Kunming Institute of Zoology, Chinese Academy of Sciences (approval ID SMKX-2018018). All possible efforts were made to reduce the sample size and also to minimize animal suffering.

Data Availability. All data needed to evaluate the conclusions are present in this paper and/or the supporting information. Additional data are available from the authors upon request. Sequencing data (accession no. PRJNA600306) of mouse trigeminal ganglions have been deposited in the National Center for Biotechnology Information Sequence Read Archive. To record the cold-driven activation, the cells expressing TRPM8 were first placed and recorded in a 37 °C bath solution. To ensure accuracy in monitoring of the local temperature, a TA-29 miniature bead thermistor (Harvard Apparatus) was placed right next to the pipette. Briefly, a detailed version of this study's materials and methods for the transient transfection, gene synthesis, mutation, molecular modeling, fluorescence imaging, and electrophysiological measurements is provided in *SI Appendix*. These assays were all performed using standard approaches.

ACKNOWLEDGMENTS. This work was supported by funding from the National Science Foundation of China grant (331372208), Chinese Academy of Sciences grants (XDB31020303 and QYZDJ-SSW-SMC012), and Yunnan Province grant (2015HA023) (to R.L.) and from the National Science Foundation of China grants (31640071 and 31770835), Chinese Academy of Sciences (Youth Innovation Promotion Association and "Light of West China" Program), and Yunnan Province grants (2017FB037, 2018FA003, and 2019FI005) (to S.Y.). This work was also supported by funding from the National Science Foundation of China grants (31741067, 31800990, and 31971040) and Zhejiang Provincial Natural Science Foundation of China grant (LR20C050002) (to F.Y.).

1. A. Dhaka, V. Viswanath, A. Patapoutian, Trp ion channels and temperature sensation. *Annu. Rev. Neurosci.* **29**, 135–161 (2006).
2. Arizona State University, World Meteorological Organization's World Weather & Climate Extremes Archive. https://wmo.asu.edu/#global. Accessed 1 October 2019.
3. S. Saito, M. Tominaga, Evolutionary tuning of TRPA1 and TRPV1 thermal and chemical sensitivity in vertebrates. *Temperature* **4**, 141–152 (2017).
4. W. J. Laursen, E. R. Schneider, D. K. Merriman, S. N. Bagriantsev, E. O. Gracheva, Low-cost functional plasticity of TRPV1 supports heat tolerance in squirrels and camels. *Proc. Natl. Acad. Sci. U.S.A.* **113**, 11342–11347 (2016).
5. V. Matos-Cruz *et al*., Molecular prerequisites for diminished cold sensitivity in ground squirrels and hamsters. *Cell Rep.* **21**, 3329–3337 (2017).
6. D. D. McKemy, W. M. Neuhausser, D. Julius, Identification of a cold receptor reveals a general role for TRP channels in thermosensation. *Nature* **416**, 52–58 (2002).
7. A. M. Peier *et al*., A TRP channel that senses cold stimuli and menthol. *Cell* **108**, 705–715 (2002).
8. A. Dhaka *et al*., TRPM8 is required for cold sensation in mice. *Neuron* **54**, 371–378 (2007).
9. M. M. Moran, TRP channels as potential drug targets. *Annu. Rev. Pharmacol. Toxicol.* **58**, 309–330 (2018).
10. S. Brauchi, G. Orta, M. Salazar, E. Rosenmann, R. Latorre, A hot-sensing cold receptor: C-terminal domain determines thermosensation in transient receptor potential channels. *J. Neurosci.* **26**, 4835–4840 (2006).
11. M. Pertusa, B. Rivera, A. González, G. Ugarte, R. Madrid, Critical role of the pore domain in the cold response of TRPM8 channels identified by ortholog functional comparison. *J. Biol. Chem.* **293**, 12454–12471 (2018).
12. Y. Yin *et al*., Structure of the cold- and menthol-sensing ion channel TRPM8. *Science* **359**, 237–241 (2018).
13. Y. Yin *et al*., Structural basis of cooling agent and lipid sensing by the cold-activated TRPM8 channel. *Science* **363**, eaav9334 (2019).
14. M. M. Diver, Y. F. Cheng, D. Julius, Structural insights into TRPM8 inhibition and desensitization. *Science* **365**, 1434–1440 (2019).
15. F. Yang, Y. Cui, K. Wang, J. Zheng, Thermosensitive TRP channel pore turret is part of the temperature activation pathway. *Proc. Natl. Acad. Sci. U.S.A.* **107**, 7083–7088 (2010).
16. S. Brauchi, P. Orio, R. Latorre, Clues to understanding cold sensation: Thermodynamics and electrophysiological analysis of the cold receptor TRPM8. *Proc. Natl. Acad. Sci. U.S.A.* **101**, 15494–15499 (2004).
17. D. E. Clapham, C. Miller, A thermodynamic framework for understanding temperature sensing by transient receptor potential (TRP) channels. *Proc. Natl. Acad. Sci. U.S.A.* **108**, 19492–19497 (2011).
18. S. Chowdhury, B. W. Jarecki, B. Chanda, A molecular framework for temperature-dependent gating of ion channels. *Cell* **158**, 1148–1158 (2014).
19. B. R. Myers, Y. M. Sigal, D. Julius, Evolution of thermal response properties in a cold-activated TRP channel. *PLoS One* **4**, e5741 (2009).

20. T. Voets *et al*., The principle of temperature-dependent gating in cold- and heat-sensitive TRP channels. *Nature* **430**, 748–754 (2004).
21. A. Chatterjee, J. Guo, H. S. Lee, P. G. Schultz, A genetically encoded fluorescent probe in mammalian cells. *J. Am. Chem. Soc.* **135**, 12540–12543 (2013).
22. F. Yang *et al*., The conformational wave in capsaicin activation of transient receptor potential vanilloid 1 ion channel. *Nat. Commun.* **9**, 2879 (2018).
23. L. Luo *et al*., Molecular basis for heat desensitization of TRPV1 ion channels. *Nat. Commun.* **10**, 2134 (2019).
24. T. Hessa *et al*., Recognition of transmembrane helices by the endoplasmic reticulum translocon. *Nature* **433**, 377–381 (2005).
25. C. P. Moon, K. G. Fleming, Side-chain hydrophobicity scale derived from transmembrane protein folding into lipid bilayers. *Proc. Natl. Acad. Sci. U.S.A.* **108**, 10174–10177 (2011).
26. C. Zhu *et al*., Characterizing hydrophobicity of amino acid side chains in a protein environment via measuring contact angle of a water nanodroplet on planar peptide network. *Proc. Natl. Acad. Sci. U.S.A.* **113**, 12946–12951 (2016).
27. M. B. Ulmschneider, M. S. P. Sansom, A. Di Nola, Properties of integral membrane protein structures: Derivation of an implicit membrane potential. *Proteins* **59**, 252–265 (2005).
28. C. A. Schramm *et al*., Knowledge-based potential for positioning membrane-associated structures and assessing residue-specific energetic contributions. *Structure* **20**, 924–935 (2012).
29. A. Senes *et al*., E(z), a depth-dependent potential for assessing the energies of insertion of amino acid side-chains into membranes: Derivation and applications to determining the orientation of transmembrane and interfacial helices. *J. Mol. Biol.* **366**, 436–448 (2007).
30. H. Nakashima, K. Nishikawa, The amino acid composition is different between the cytoplasmic and extracellular sides in membrane proteins. *FEBS Lett.* **303**, 141–146 (1992).
31. W. M. Yau, W. C. Wimley, K. Gawrisch, S. H. White, The preference of tryptophan for membrane interfaces. *Biochemistry* **37**, 14713–14718 (1998).
32. M. Levitt, A simplified representation of protein conformations for rapid simulation of protein folding. *J. Mol. Biol.* **104**, 59–107 (1976).
33. T. P. Hopp, K. R. Woods, Prediction of protein antigenic determinants from amino-acid-sequences. *Proc. Natl. Acad. Sci. U.S.A.* **78**, 3824–3828 (1981).
34. R. M. Sweet, D. Eisenberg, Correlation of sequence hydrophobicities measures similarity in three-dimensional protein structure. *J. Mol. Biol.* **171**, 479–488 (1983).
35. S. Miyazawa, R. L. Jernigan, Estimation of effective interresidue contact energies from protein crystal-structures—Quasi-chemical approximation. *Macromolecules* **18**, 534–552 (1985).
36. T. Ooi, M. Oobatake, G. Némethy, H. A. Scheraga, Accessible surface areas as a measure of the thermodynamic parameters of hydration of peptides. *Proc. Natl. Acad. Sci. U.S.A.* **84**, 3086–3090 (1987).
37. M. Oobatake, T. Ooi, Characteristic thermodynamic properties of hydrated water for 20 amino acid residues in globular proteins. *J. Biochem.* **104**, 433–439 (1988).
38. D. M. Bautista *et al*., The menthol receptor TRPM8 is the principal detector of environmental cold. *Nature* **448**, 204–208 (2007).
39. R. W. Colburn *et al*., Attenuated cold sensitivity in TRPM8 null mice. *Neuron* **54**, 379–386 (2007).
40. N. Raddatz, J. P. Castillo, C. Gonzalez, O. Alvarez, R. Latorre, Temperature and voltage coupling to channel opening in transient receptor potential melastatin 8 (TRPM8). *J. Biol. Chem.* **289**, 35438–35454 (2014).
41. J. Zheng, Molecular mechanism of TRP channels. *Compr. Physiol.* **3**, 221–242 (2013).
42. J. Zheng, L. Ma, Structure and function of the thermoTRP channel pore. *Curr. Top. Membr.* **74**, 233–257 (2014).
43. F. Yang *et al*., Structural mechanism underlying capsaicin binding and activation of the TRPV1 ion channel. *Nat. Chem. Biol.* **11**, 518–524 (2015).
44. F. Zhang *et al*., Heat activation is intrinsic to the pore domain of TRPV1. *Proc. Natl. Acad. Sci. U.S.A.* **115**, E317–E324 (2018).
45. J. Grandl *et al*., Temperature-induced opening of TRPV1 ion channel is stabilized by the pore domain. *Nat. Neurosci.* **13**, 708–714 (2010).
46. J. Grandl *et al*., Pore region of TRPV3 ion channel is specifically required for heat activation. *Nat. Neurosci.* **11**, 1007–1013 (2008).
47. A. Jara-Oseguera, K. E. Huffer, K. J. Swartz, The ion selectivity filter is not an activation gate in TRPV1-3 channels. *Elife* **8**, e51212 (2019).
48. J. O. Sosa-Pagán, E. S. Iversen, J. Grandl, TRPV1 temperature activation is specifically sensitive to strong decreases in amino acid hydrophobicity. *Sci. Rep.* **7**, 549 (2017).
49. G. M. Story *et al*., ANKTM1, a TRP-like channel expressed in nociceptive neurons, is activated by cold temperatures. *Cell* **112**, 819–829 (2003).
50. J. Chen *et al*., Species differences and molecular determinant of TRPA1 cold sensitivity. *Nat. Commun.* **4**, 2501 (2013).